Supplemental material

Shivange et al., https://doi.org/10.1085/jgp.201812201

Amine-containing buffers produce anomalous results

With Tris or HEPES buffers, experiments on purified iNicSnFRs gave elevated F_0 values and decreased ΔF values, compared with phosphate buffers. Isothermal titration calorimetry experiments with Tris buffers gave affinities much lower than with phosphate-containing buffers. We found similar anomalies with MOPS at >10 mM.

In experiments on purified iNicSnFR proteins, like those of Fig. 3, MOPS buffer at ≤10 mM produced minimal perturbation. However, live-cell experiments with MOPS and iNicSnFR3a_ER gave anomalously low $\Delta F/F_0$, probably because this buffer allowed the ER to become acidic.

Use of HEPES might have degraded the quality of the crystallographic data showing nicotine at the binding site. Even slight affinity to the buffer molecule might produce competition with the desired ligand. Examples of crystallized protein containing the amine buffer, rather than nicotine, ACh, or choline, are provided by the studies of ACh-binding protein (Brejc et al., 2001; PDB file 1I9B) and of ProX (Tschapek et al., 2011; PDB file 3MAM).

Acidic vesicles as candidates for the "sequestered compartment"

Our simulations include a "sequestered" compartment. This was previously termed a "peripheral" compartment (Benowitz et al., 1991), but the previous terminology would introduce confusion about nicotine in the peripheral nervous system. Wording aside, where is this sequestered compartment, whose chief characteristic is that it remains inaccessible from metabolic enzymes? Early on, it was pointed out (de Duve et al., 1974) that weak bases accumulate, perhaps by factors of 100, in lysosomes or other acidic compartments. In 2009, it was suggested that nicotine could also become concentrated in this fashion (Lester et al., 2009). The pharmacokinetic literature points out that lysosomes (pH ∼4.5), representing just ∼1% of a cell's volume, but concentrating a weakly basic drug by ∼100-fold, could accumulate as much drug as the entire cellular and extracellular compartments (Smith et al., 2012). Tischbirek et al. (2012) provided experimental evidence that antipsychotic drugs, which are also weak bases, accumulate in synaptic vesicles (pH ∼5.5) and also presented a quantitative analysis including the dependence on logD and membrane permeation of the protonated, charged form (Trapp et al., 2008; Tischbirek et al., 2012). These concepts strengthen the recent suggestion that varenicline accumulates in lysosomes (Govind et al., 2017).

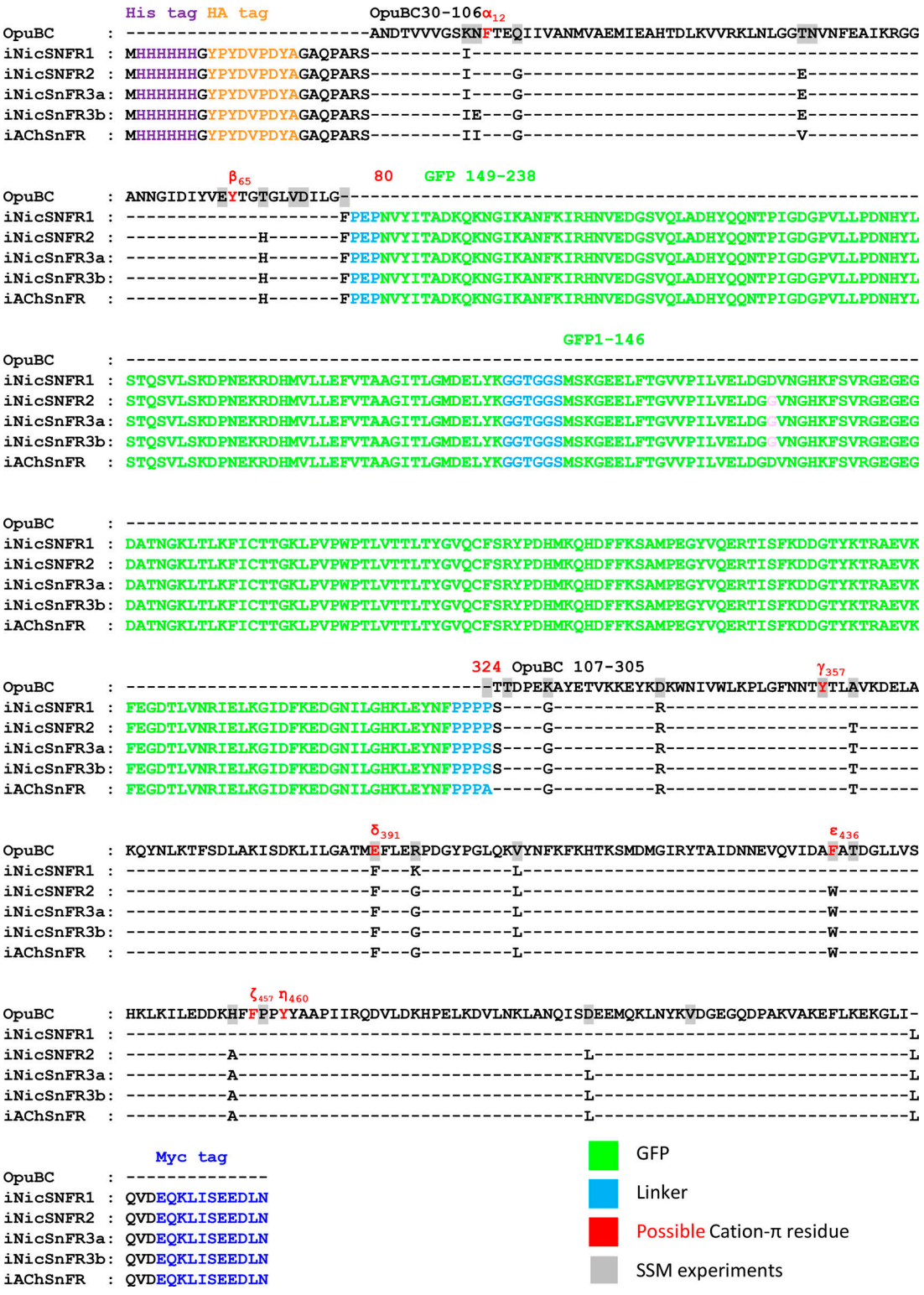

Figure S1. **Sequences of PBPs and constructs described in this paper and/or studied in preliminary experiments.** The nicotine dose–response characteristics of iNicSnFR1 and iNicSnFR2 biosensors are given in Fig. S2 B. These constructs have not been studied systematically in mammalian cells with optimized methods. Experiments with iAChSnFR are described elsewhere (Borden et al., in preparation). Important domains are noted on the sequences. Based on a SwissDock simulation of nicotine in iNicSnFR1 (see Fig. 2 B), we have annotated the seven aromatic residues within 5 Å of the pyrrolidine nitrogen in nicotine. These are labeled α through η. One or more of these side chains may be involved in a cation-π interaction with the protonated pyrrolidine moiety of nicotine, with the quaternary amine of N'MeNic, and/or with the secondary amine of varenicline (Tavares et al., 2012; Post et al., 2017). The OpuBC sequence is annotated with a gray background at the 25 codons we subjected to SSM experiments. In communications among the collaborators on this project, we have used the following additional descriptions and temporary names. For iNicSNFR1: CC47, V4.6. For iNicSNFR2: CC90. For iNicSnFR3a: CC93. For iNicSnFR3a_Y357A_PM: CC105. For iNicSnFR3b: V7. For iAChSnFR: V9.

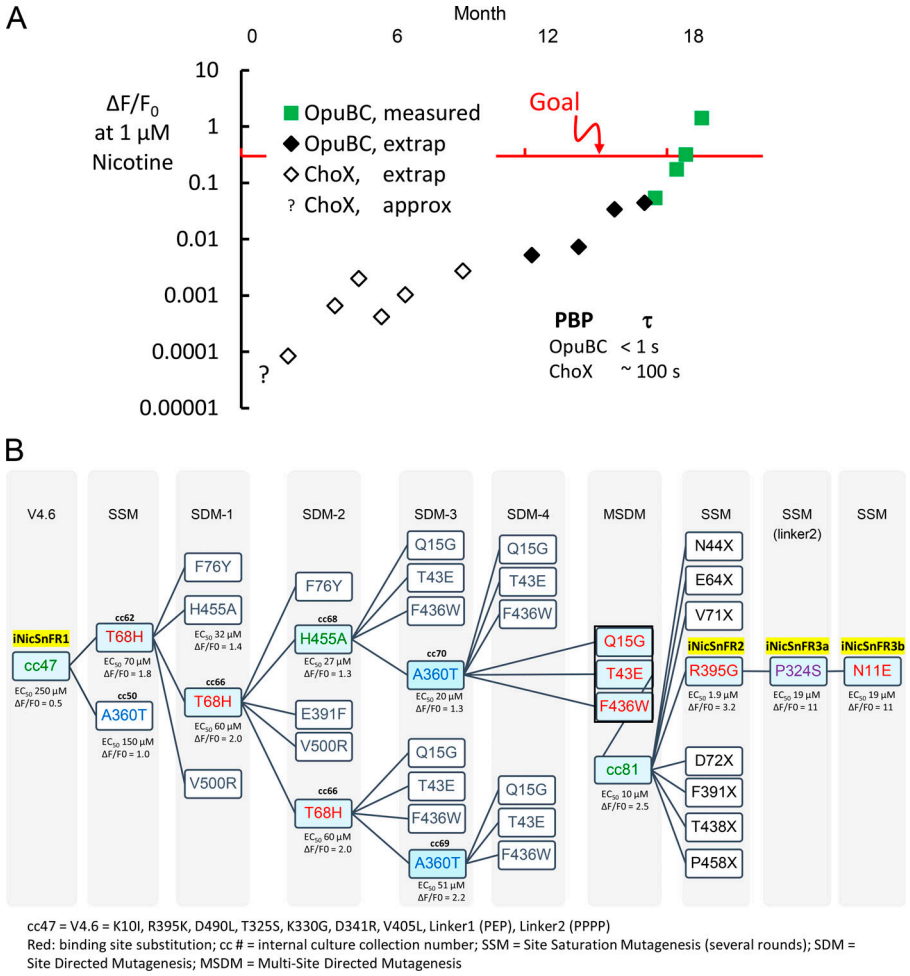

Figure S2. **Directed evolution of the iNicSnFR family. (A)** A history of our progress toward the goal of $\Delta F/F_0$ > 0.3 at 1 µM nicotine. Initial experiments used ChoX, a choline PBP from *Sinorhizobium meliloti*. However, these constructs responded to ligands in solution with a time constant of τ > 100 s and were also poorly expressed in mammalian cells. We ceased systematic development of ChoX-based constructs. Later experiments used OpuBC from *T. spX513*, as described in the text and in Fig. 2. The reported values were measured in *Escherichia coli* cell lysates; values for key constructs were later verified with samples of the purified proteins. **(B)** Final stages in protein engineering of iNicSnFR constructs. For constructs denoted by black or white symbols, $\Delta F/F_0$ at >1 µM nicotine was extrapolated from measurements on bacterial lysates as $[\Delta F/F_{max}]/EC_{50}$. For constructs denoted by green symbols, $\Delta F/F_0$ at 0.3 µM nicotine was measured directly on bacterial lysates. The designs of the mutant libraries were based on the iNicSnFR1 structure depicted in Fig. 2 A and the docking results of Fig. 2 B. The sites selected for mutagenesis include the nicotine-binding pocket, linker residues, and the interface between OpuBC and cpGFP. Interestingly, the substitution A360T improved affinity despite its location "far" from the binding pocket (on a β-sheet next to one of the active site loops). The site A360 was selected based on the crystal structure of ACh-binding protein (AChBP) in complex with nicotine (PDB file 1UW6). Additional names for communications among collaborators are given in Fig. S1. Red: binding site substitution. Techniques: site saturation mutagenesis (several rounds), site-directed mutagenesis, and multisite-directed mutagenesis.

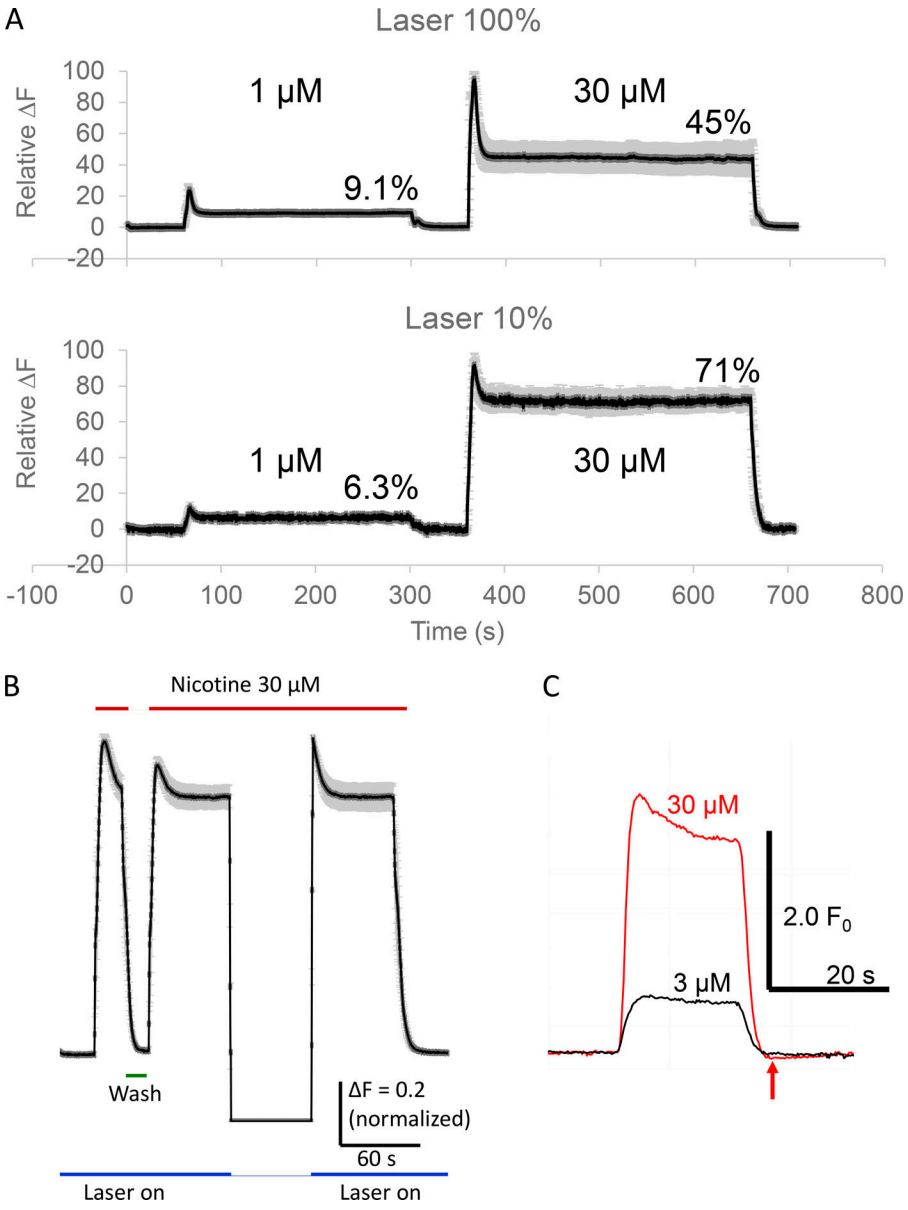

Figure S3. **Photoswitching (bleaching) is noticeable at high [nicotine] with focused laser illumination. (A)** Photoswitching (bleaching) increases at the highest illumination intensities and at higher [nicotine]. HeLa cells transfected with iNicSnFR3a_PM. Imaging at 1 and 30 µM nicotine, with 100% and 10% laser intensity (top and bottom, respectively). At 30 µM nicotine, photoswitching reduced the steady-state ΔF to 45 versus 71% of the peak ΔF for 100% and 10% laser intensity, respectively. The steady-state ratio, ΔF(30 µM) to ΔF(1 µM) was 4.92 versus 11.2 for 100% and 10%, respectively, indicating that high intensities artifactually shifted the dose–response relation ([nicotine] vs. ΔF) to lower [nicotine]. Traces are mean ± SEM; three cells. At 30 µM nicotine, photoswitching also proceeded more rapidly for 100% than for 10% intensity (time constant, 3.47 vs. 5.55 s, respectively). At 1 µM nicotine, data were too noisy for systematic kinetic studies. **(B)** Photoswitching is reversible. HeLa cells transfected with iNicSnFR3a_PM, imaging at 30 µM nicotine. During an initial 20-s nicotine application, ΔF reaches a peak, then decreases. During a second 200-s application, ΔF reaches a peak, then recovers to a plateau. The laser is switched off for 60 s during the continued presence of nicotine. When the laser is switched on again, ΔF appears to have recovered to its initial peak, then bleaches to its former plateau. Traces are normalized from five cells, and the gray bands show ± SEM. **(C)** Further analysis of reversible photoswitching. HeLa cells transfected with iNicSnFR3a_ER. Experiment at 100% laser intensity, 30 µM versus 3 µM nicotine. When 30 µM nicotine is removed, the trace reveals a transient decrease in F_0 (red arrow). In the absence of nicotine, when iNicSnFR is absorbing fewer photons, F_0 recovers to its unbleached state over the next 10 s. Photoswitching was not observed with LED illumination.

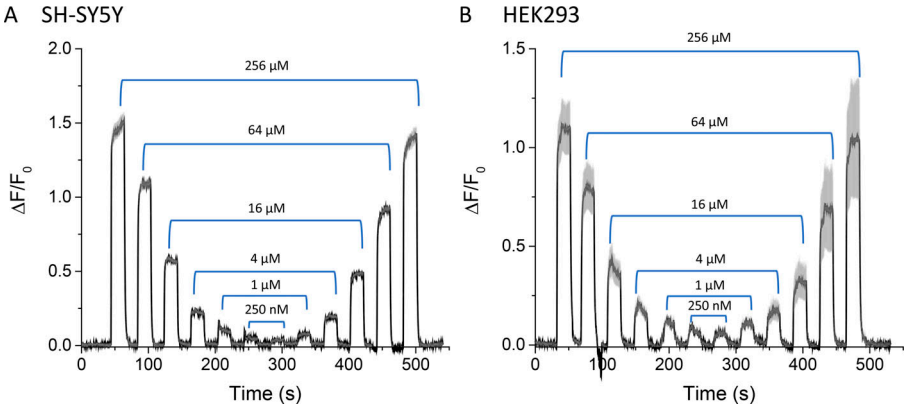

Figure S4. **Responses to nicotine with iNicSnFR_ER in SH-SY5Y cells and HEK293 cells. (A and B)** iNicSnFR_ER was transfected and imaged in SH-SY5Y (A) and HEK293 cells (B). Nicotine pulses were applied for 20 s at 40-s intervals. The nicotine concentration was stepped from 256 µM to 250 nM and then from 250 nM to 256 µM in 4× concentration steps in HBSS. The mean of three cells is given as a solid black line, and the SEM is given as gray bounds.

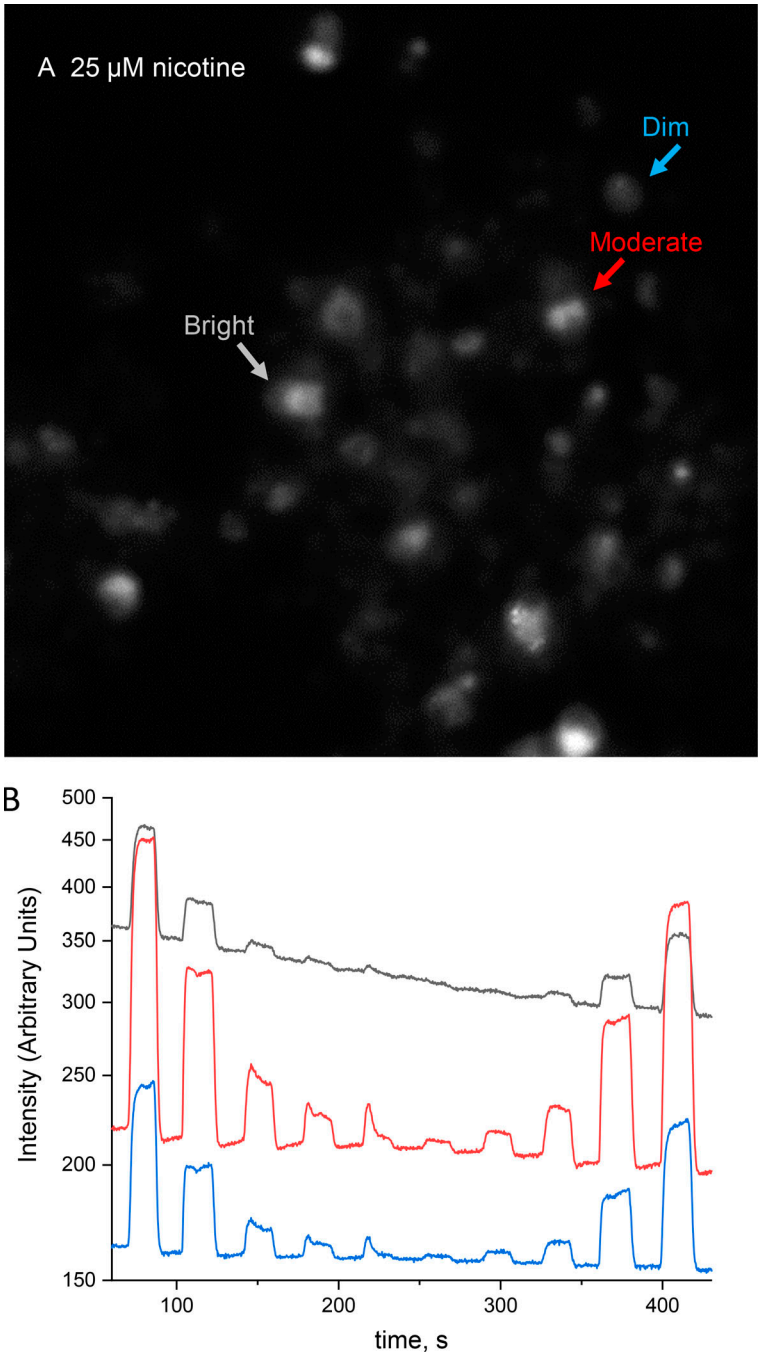

Figure S5. **Human iPSCs, differentiated to dopaminergic neurons, transduced with AAV_iNicSnFR3b_ER.** This figure accompanies the video of a descending, then ascending, series of nicotine concentrations at fivefold steps between 0.2 and 125 µM. Concentrations and washes ("0 µM") are marked on the video. **(A)** The image shows a single frame taken at 25 µM nicotine, indicating three cells (dim, moderate, and bright). **(B)** Plots of the average absolute intensity of these images (log scale), without correction for sloping baseline or conversion to $\Delta F/F_0$. Note that in the descending phase, the responses begin more quickly and, at the lower [nicotine], show an initial transient. This is an artifactual result when solutions in a pH-regulated reservoir are allowed to remain in gas-permeable intermediate tubing, allowing CO_2 to escape and rendering the solutions slightly more basic (see Materials and methods). The second application of each solution utilizes solution that has recently moved from the larger reservoir; the transients no longer appear.

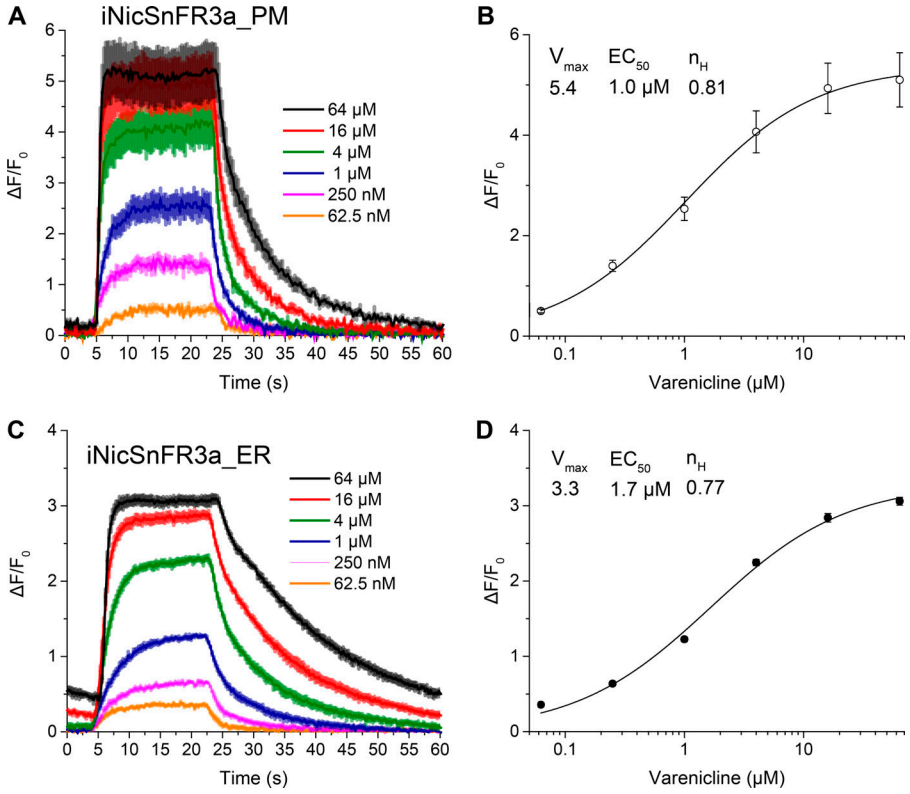

Figure S6. **Varenicline at iNicSnFR3a expressed in HeLa cells. (A and C)** Dose–response relations for varenicline-induced $\Delta F/F_0$. Mean ± SEM; three measurements. **(B and D)** Dose–response plots for $\Delta F/F_0$ at each response in A and C, against [varenicline]. Single-component Hill equation fit, including zero response at zero [varenicline]. Parameter values are shown.

Table S1. **Structure and refinement of iNicSnFR1 crystallized with nicotine**

Wavelength, Å	1.541
Resolution range, Å	61.64–2.4 (2.486–2.4)
Space group	I 2 2 2
Unit cell, Å	80.61, 95.64, 151.79, 90, 90, 90
Total reflections	758,695 (72898)
Unique reflections	23,162 (2253)
Multiplicity	32.8 (32.3)
Completeness, %	99.07 (98.82)
Mean I/σ(I)	47.79 (3.74)
Wilson B-factor	36.67
R_{merge}	0.749 (1.909)
R_{meas}	0.761 (1.939)
R_{pim}	0.133 (0.342)
$CC_{1/2}$	0.924 (0.737)
CC*	0.98 (0.921)
Reflections used in refinement	23,132 (2253)
Reflections used for R-free	1178 (100)
R_{work}	0.1902 (0.2311)
R_{free}	0.2521 (0.3714)
CC_{work}	0.878 (0.811)
CC_{free}	0.828 (0.381)
Number of non-hydrogen atoms	4,042
macromolecules	3,989
ligands	22
solvent	31
Protein residues	504
RMS deviation, bonds	0.009
RMS deviation angles	1.36
Ramachandran plot: favored %	95.56
Allowed %	4.44
Outliers %	0.00
Rotamer outliers %	0.23
Clash score	10.25
Average B-factor	45.07
macromolecules	45.17
ligands	29.03
solvent	42.60
Number of TLS groups	4

Statistics for the highest-resolution shell are shown in parentheses.

Table S2. **Parameters for nicotine and varenicline Matlab/SimBiology models.**

	Parameter Name	Nicotine		Varenicline	
		Value	References	Value	References
Volume of distribution	Vd	200 liters	Benowitz et al. (1991)	420 liters	Faessel et al. (2006)
EC_{50} for activating PM nAChR receptor channels	Activation k−/k+	1,000 nM		3,000 nM	Coe et al. (2005); Rollema et al. (2007)
EC_{50} for chaperoning ER nAChR proteins	Chaperoning k−/k+	37 nM	Kuryatov et al. (2005)	10 nM	Govind et al. (2017)
PM nAChR Concentration	PM nAChR	0.1 nM		0.1 nM	
ER nAChR Concentration	ER nAChR	0.1 nM		0.1 nM	
Elimination rate constant	kel	0.706 1/h	Benowitz et al. (1991)	2.6 1/h	Rollema et al. (2010)
Rate constant, Plasma/CSF/ER to sequestered	kf	1.5 1/h	Benowitz et al. (1991)	0.6 1/h	Rollema et al. (2010)
Rate constant, sequestered to Plasma/CSF/ER	kr	1.2 1/h	Benowitz et al. (1991)	2.5 1/h	Rollema et al. (2010)
Absorption rate constant	ka_available	N/A		1.035 1/h	Rollema et al. (2010)
Bioavailability	F	1		0.9	US Food and Drug Administration (2011)

Assumed Vd: 2.86 liter/kg, 6 liter/kg; 70 kg person

Table S3. **Supplemental videos**

Cell type	Drug	MP4 file number	Expression construct, LED voltage, Concentrations (if not labelled in the video)	Total time, s	Drug additions, s	Speed vs real time (fold)
iDopaNeurons (iPSCs)	Nicotine	1	AAV2-iNicSnFR3b_ER, 17days, 120mV, 125-25-5-1-0.2 µM	193	20	5.9
HeLa cells	Nicotine	2	iNicSnFR3a_PM, 30mV	285	20	9.5
		3	iNicSnFR_ER,30mV	289	20	9.6
	Varenicline	4	iNicSnFR3a, PM, 30mV	401	30	12.9
		5	iNicSnFR3a_ER, 30mV	396	30	13.2
Hippocampal Cultures	Nicotine	6	AAV2-iNicSnFR3b_ER, 62mV	342	20	12.2
		7	AAV2-iNicSnFR3b_PM, 125mV	335	20	12
	Varenicline	8	AAV2-iNicSnFRb_PM, 180mV	569	20	16.7
		9	AAV2-iNicSnFR3b_ER, 16mV	564	20	17.1

Each video is colored using the "fire" lookup table (blue < red < white). The lookup table is constant across the field and within each video, so that cells with varying levels of iNicSnFRs begin with varying colors. The general procedure is a series of steps in concentration of a single drug (either nicotine or varenicline), separated by control solution. Field of view is 211-µM wide. Please begin with Video 1 (nicotine). Its annotation is most complete, and it shows a "descending-increasing" series of nicotine concentrations. Figure S5 is a frame from this movie.

References

Benowitz, N.L., P. Jacob III, C. Denaro, and R. Jenkins. 1991. Stable isotope studies of nicotine kinetics and bioavailability. *Clin. Pharmacol. Ther.* 49:270–277. https://doi.org/10.1038/clpt.1991.28

Brejc, K., W.J. van Dijk, R.V. Klaassen, M. Schuurmans, J. van Der Oost, A.B. Smit, and T.K. Sixma. 2001. Crystal structure of an ACh-binding protein reveals the ligand-binding domain of nicotinic receptors. *Nature.* 411:269–276. https://doi.org/10.1038/35077011

Coe, J.W., P.R. Brooks, M.G. Vetelino, M.C. Wirtz, E.P. Arnold, J. Huang, S.B. Sands, T.I. Davis, L.A. Lebel, C.B. Fox, et al. 2005. Varenicline: an α4β2 nicotinic receptor partial agonist for smoking cessation. *J. Med. Chem.* 48:3474–3477. https://doi.org/10.1021/jm050069n

de Duve, C., T. de Barsy, B. Poole, A. Trouet, P. Tulkens, and F. Van Hoof. 1974. Commentary. Lysosomotropic agents. *Biochem. Pharmacol.* 23:2495–2531. https://doi.org/10.1016/0006-2952(74)90174-9

Faessel, H.M., M.A. Gibbs, D.J. Clark, K. Rohrbacher, M. Stolar, and A.H. Burstein. 2006. Multiple-dose pharmacokinetics of the selective nicotinic receptor partial agonist, varenicline, in healthy smokers. *J. Clin. Pharmacol.* 46:1439–1448. https://doi.org/10.1177/0091270006292624

Govind, A.P., Y.F. Vallejo, J.R. Stolz, J.Z. Yan, G.T. Swanson, and W.N. Green. 2017. Selective and regulated trapping of nicotinic receptor weak base ligands and relevance to smoking cessation. *eLife.* 6:e25651. https://doi.org/10.7554/eLife.25651

Kuryatov, A., J. Luo, J. Cooper, and J. Lindstrom. 2005. Nicotine acts as a pharmacological chaperone to up-regulate human α4β2 acetylcholine receptors. *Mol. Pharmacol.* 68:1839–1851.

Lester, H.A., C. Xiao, R. Srinivasan, C.D. Son, J. Miwa, R. Pantoja, M.R. Banghart, D.A. Dougherty, A.M. Goate, and J.C. Wang. 2009. Nicotine is a selective pharmacological chaperone of acetylcholine receptor number and stoichiometry. Implications for drug discovery. *AAPS J.* 11:167–177. https://doi.org/10.1208/s12248-009-9090-7

Post, M.R., H.A. Lester, and D.A. Dougherty. 2017. Probing for and Quantifying Agonist Hydrogen Bonds in α6β2 Nicotinic Acetylcholine Receptors. *Biochemistry.* 56:1836–1840. https://doi.org/10.1021/acs.biochem.7b00213

Rollema, H., L.K. Chambers, J.W. Coe, J. Glowa, R.S. Hurst, L.A. Lebel, Y. Lu, R.S. Mansbach, R.J. Mather, C.C. Rovetti, et al. 2007. Pharmacological profile of the α4β2 nicotinic acetylcholine receptor partial agonist varenicline, an effective smoking cessation aid. *Neuropharmacology.* 52:985–994. https://doi.org/10.1016/j.neuropharm.2006.10.016

Rollema, H., A. Shrikhande, K.M. Ward, F.D. Tingley III, J.W. Coe, B.T. O'Neill, E. Tseng, E.Q. Wang, R.J. Mather, R.S. Hurst, et al. 2010. Pre-clinical properties of the α4β2 nicotinic acetylcholine receptor partial agonists varenicline, cytisine and dianicline translate to clinical efficacy for nicotine dependence. *Br. J. Pharmacol.* 160:334–345. https://doi.org/10.1111/j.1476-5381.2010.00682.x

Smith, D., C. Allerton, A. Kalgutkar, H. van de Waterbeemd, and D. Walker, editors. 2012. *Pharmacokinetics and Metabolism in Drug Design.* Third edition. Wiley, Weinheim, Germany. 268 pp. https://doi.org/10.1002/9783527645763

Tavares, X.S., A.P. Blum, D.T. Nakamura, N.L. Puskar, J.A. Shanata, H.A. Lester, and D.A. Dougherty. 2012. Variations in binding among several agonists at two stoichiometries of the neuronal, α4β2 nicotinic receptor. *J. Am. Chem. Soc.* 134:11474–11480. https://doi.org/10.1021/ja3011379

Tischbirek, C.H., E.M. Wenzel, F. Zheng, T. Huth, D. Amato, S. Trapp, A. Denker, O. Welzel, K. Lueke, A. Svetlitchny, et al. 2012. Use-dependent inhibition of synaptic transmission by the secretion of intravesicularly accumulated antipsychotic drugs. *Neuron.* 74:830–844. https://doi.org/10.1016/j.neuron.2012.04.019

Trapp, S., G.R. Rosania, R.W. Horobin, and J. Kornhuber. 2008. Quantitative modeling of selective lysosomal targeting for drug design. *Eur. Biophys. J.* 37:1317–1328. https://doi.org/10.1007/s00249-008-0338-4

Tschapek, B., M. Pittelkow, L. Sohn-Bösser, G. Holtmann, S.H. Smits, H. Gohlke, E. Bremer, and L. Schmitt. 2011. Arg149 is involved in switching the low affinity, open state of the binding protein AfProX into its high affinity, closed state. *J. Mol. Biol.* 411:36–52. https://doi.org/10.1016/j.jmb.2011.05.039

US Food and Drug Administration. 2011. Chantix package insert. https://www.accessdata.fda.gov/drugsatfda_docs/label/2011/021928s025lbl.pdf.